Optimisation of single-nuclei isolation and RNA sequencing of parasitic nematodes

Sarah K Buddenborg[1], Alison A Morrison[3], Anna C Fletcher[1], Manuela R Kieninger[1], Bee Ling Ng[1], Kirsty Maitland[2], Emily Hart[4], Dave J Bartley[3], Maria A Duque-Correa[4], Stephen R Doyle[1]

[1]**Wellcome Sanger Institute, Hinxton, Cambridgeshire, CB10 1SA, UK**
Sarah K Buddenborg (sarah.buddenborg@sanger.ac.uk)
Anna C Fletcher (annie.fletcher@sanger.ac.uk)
Manuela R Kieninger (manuela.kieninger@sanger.ac.uk)
Bee Ling Ng (beeling.ng@sanger.ac.uk)
Stephen R Doyle (stephen.doyle@sanger.ac.uk)

[2]**University of Glasgow, SBOHVM, Garscube Campus, G61 1QH**
Kirsty Maitland (kirsty.maitland@glasgow.ac.uk)

[3]**Moredun Research Institute, Pentlands Science Park, Bush Loan, Penicuik, EH26 0PZ, UK**
Alison A Morrison (alison.morrison@moredun.ac.uk)
Dave J Bartley (dave.bartley@moredun.ac.uk)

[4]**Cambridge Stem Cell Institute, University of Cambridge, Cambridge, CB2 0AW, UK**
Emily Hart (ejh200@cam.ac.uk)
Maria A Duque-Correa (mad75@cam.ac.uk)

Abstract

Single-cell/nuclei transcriptomics has revolutionised our understanding of cell, tissue, and organismal biology during health and disease of humans and model organisms. However, for non-model species, reassessment and refinement of conventional methods to address novel technical and biological challenges are needed. Here, we evaluate three established nuclei isolation protocols and, building on experiences, optimised single nuclei isolation for parasitic nematodes (SNIP). We test the versatility of SNIP across diverse species and life stages, validating it with snRNA-seq to reveal sex, stage, and tissue-specific gene expression. Optimised protocols will advance the understanding of parasitic nematodes, from fundamental biology to infection and disease.

Keywords

Single-nuclei RNA-seq, nematodes, helminths, transcriptomics, protocol optimisation

Introduction

With the increasing affordability and availability of high-throughput sequencing and commercial single-cell (sc) and single-nuclei (sn) transcriptomic platforms, cellular-resolution approaches to investigate the biology of non-model organisms are becoming more accessible. Applying sc/snRNA-seq to non-model organisms does, however, bring new biological and technical challenges that may need to be overcome. For example, the biological richness of non-model organism diversity brings a diversity of cell and tissue types that vary in their morphology and composition and will differ in their sensitivities toward cellular and nuclei dissociation. Further, sample access may be impacted by geographic or biological constraints, limiting the availability of or access to fresh material. Understanding and overcoming these challenges will likely require organism-specific biological knowledge. Therefore, conventional, well-established methods developed for model organisms may need adaptation and refinement for use in non-model organisms.

A field with exclusively non-model organisms that stands to benefit greatly from understanding biology at a single-cell resolution is parasitology. scRNA-seq of single-cell eukaryotic parasites such as *Plasmodium spp.* and *Trypanosoma spp.* has been particularly successful, with significant advances made in understanding life stage-specific gene expression patterns and transitions during their life cycles, mechanisms of infection and

disease progression, as well as identifying new drug targets for interrupting transmission [1–7]. In contrast, the application of scRNA-seq for multicellular parasites has encountered distinct challenges due to vast differences in life history traits and hosts and great diversity in body plan and cellular composition between and even within species throughout their life cycles. Multicellular parasites are exposed to variable environmental conditions inside and outside the host, necessitating a toughened outer coating (i.e. cuticle, tegument, exoskeleton), which presents a major obstacle for single-cell/nuclei isolation. Further, because most species cannot be cultured *in vitro*, access to obligate parasitic stages can be geographically restricted and difficult or impossible to collect without sampling post-mortem. Despite these challenges, there are a growing number of single-cell life-stage atlases for parasitic helminths, including the trematodes *Schistosoma mansoni* [8–11] and *Fasciola hepatica* [12]. More recently, cell atlases have been generated for *Brugia malayi* microfilariae [13], *Ascaris suum* intestinal tissue [14], *Haemonchus contortus* embryos [15], and *Heligmosomoides bakeri* mixed-sex adults [16]. These studies often utilise protocols developed for mammalian tissues, although it is unclear how transferable and efficient these different single-cell isolation methods are for diverse species and life cycle stages of parasitic helminths.

In this study, we have tested and compared three widely used single-nuclei isolation protocols for use in snRNA-seq of parasitic nematodes. We focused on isolating single nuclei rather than single cells because frozen material can be used more readily, providing several advantages, including the ability to sample across life stages, collect and store samples over time, and process them simultaneously to minimise batch effects. Building on our experiences from the three-protocol comparison, we have developed a new nuclei isolation protocol and tested it on multiple life cycle stages and sexes of two gastrointestinal parasitic nematodes, *Haemonchus contortus* and *Trichuris muris*. We assessed the nuclei preparations from our protocol using the Parse Biosciences Evercode WT platform for snRNA-seq and Illumina sequencing. Here, we provide the protocol and discuss some of the challenges and opportunities of sc/snRNA-seq approaches to advance the adoption of this technology in non-model organisms and its applications to better understand helminth biology.

Results

Comparison of three existing nuclei isolation protocols

To optimise a protocol for generating single nuclei suspensions from parasitic nematodes, we first compared the strengths and limitations of three established isolation protocols: (i) a *Caenorhabditis elegans* nuclei isolation protocol (hereinafter referred to as "Celegans") [17,18], (ii) a Human Cell Atlas (HCA) protocol [19], and (iii) the Frankenstein protocol [20]. The Celegans protocol was the only protocol explicitly used for a nematode. The HCA protocol has been extensively used on a wide range of mammalian tissues as part of the Human Cell Atlas Project [21]. The Frankenstein protocol [20] was chosen because it was developed for use on small sample sizes and for its positive reputation amongst the 10x Genomics user community. An overview of the four key steps of the three protocols is shown in **Figure 1 A**, which includes tissue disruption, cell lysis and dissociation, homogenisation, and debris removal. Each protocol was performed using ten frozen adult female *H. contortus* worms to enable comparison between protocols.

Tissue disruption

Tissue disruption is the first stage of the process and involves breaking the tissue to reveal the cellular contents within. This step is particularly important for nematodes, which have a highly cross-linked acellular cuticle that, depending on the organism's life history or life stage, provides protection from its environment, either inside or outside a host.

The HCA and Frankenstein methods involve mincing the tissue into smaller pieces using a scalpel, while the Celegans method does not include a tissue disruption step; however, considering *C. elegans* small size (~1 mm x 50 µm), exposure of cellular contents occurs during homogenisation below.

Cell Lysis

The lysis step breaks down tissue and disrupts cellular membranes to make the nuclei accessible. The lysis buffer works in conjunction with mechanical homogenisation to create a nuclei suspension. Thus, the effectiveness of the lysis buffer, on its own, is not easily measured.

Different lysis buffers are used in each protocol, although all lysis buffer recipes typically contain the same four basic ingredients: 1) detergent to disrupt the cell membrane (e.g. Triton X-100, SDS); 2) pH stabiliser (e.g. HEPES, Tris-HCl); 3) salt to add ionic strength to

facilitate cell disruption (e.g. $MgCl_2$ $NaCl_2$, KCl); and 4) RNase inhibitor to protect RNA degradation (e.g. DTT, recombinant enzyme RNase inhibitor, EDTA). Additional RNase inhibitor was not added to the commercial lysis buffer used in the Frankenstein protocol.

Homogenisation

Homogenisation aims to completely release the cells from tissues and nuclei from cells, ensuring the suspension is free from clumps. The Celegans and HCA protocols use a glass Dounce tissue grinder to achieve a suspension of nuclei. The Celegans protocol uses ten strokes with the tight Dounce tissue grinder pestle, followed by two sets of ten strokes with a plastic micro-pestle. In between each homogenisation set, the nuclei suspension is collected using low-speed centrifugation to separate it from large undigested tissue and avoid over-homogenisation. The HCA homogenisation step required continuous homogenisation with the Dounce tissue grinder with 10-20 strokes. In contrast, the Frankenstein protocol only used a plastic micro-pestle, a 5-minute incubation in the lysis buffer, and mixing with a wide-bore pipette tip.

We examined the samples after the homogenisation stage by microscopy to determine the amount of intact tissue vs empty cuticles **(Figure 1 B)**. Empty cuticle debris was observed in the Celegans protocol, showing complete tissue homogenisation with the tight Dounce tissue grinder pestle. Large fragments of worms were prominent in the HCA and Frankenstein homogenates, indicating incomplete homogenisation.

Debris removal

The preceding steps generate significant amounts of debris, including acellular material that cannot be digested or homogenised and cellular material resulting from cell lysis. Large debris (>30 µm) can cause clogs or wetting failures in microfluidics-based library protocols, such as 10x Genomics, but presents less of a problem in combinatorial indexing strategies, where nuclei are distributed in microtiter plates. Nonetheless, small debris (<30 µm) may contain ambient RNA, increasing the transcriptional background noise [22], and should be removed.

All three protocols utilised at least one strainer for removing large debris and one wash for removing small debris. The Celegans protocol utilises low-speed centrifugation (100 g), buffer wash, and a 40 µm strainer. The HCA protocol strains the homogenate through a 40 µm filter, followed by a wash and Percoll density gradient. In the Frankenstein method, the homogenate is cleaned through a 70 µm strainer, washed, and then passed through a 35 µm strainer. Large debris was easily removed in all three protocols with cell strainers. Small

debris was observed in all three protocols but was most visually abundant in the Celegans protocol **(Figure 1 B)**. The Percoll density gradient used in the HCA protocol did not remove more small debris than the other protocols but doubled the protocol time **(Figure 1 B)**.

Outcome

The resulting nuclei suspensions of the three protocols were assessed based on the total nuclei, RNA concentration, and nuclei morphology. Using ten female *H. contortus* worms as input, the Celegans, HCA, and Frankenstein protocols resulted in a mean recovery of 7,700 ± 1,540 standard deviation (SD), 19,227 ± 3,520 SD, and 13,678 ± 1,265 SD nuclei, respectively **(Figure 1 C)**. Comparison of the three protocols revealed a significant difference between Celegans and HCA (p = 0.0065; t(4) = 5.1960), and Celegans and Frankenstein (p = 0.0065; t(4) = 5.1951), but was not statistically significant between HCA and Frankenstein (p = 0.0620; t(4) = 2.5690). Analysis of RNA concentration revealed that the Frankenstein protocol recovered the highest amount of RNA (11,790 pg) followed by the HCA and Celegans protocols (7,770 pg and 5,940 pg), respectively. The RNA concentrations were below the assay limits for reporting an RNA integrity number (RIN); however, consistent with concentration, the Frankenstein protocol presented the most prominent 18S and 28S ribosomal RNA peaks on the High Sensitivity RNA tapestation gel (**Figure 1 D**). Considering the nuclei count from the replicate used for RNA extraction from the Celegans, HCA, and Frankenstein protocols, we isolated 0.52 pg of RNA/nucleus, 0.41 pg of RNA/nucleus, and 0.81 pg of RNA/nucleus, respectively. Finally, we assessed nuclei morphology to compare suspensions from the three protocols (**Figure 1 E**). We observed notable degradation of the nuclear envelope in the Celegans protocol nuclei, which, in part, explains the poorer RNA recovery. An example of this can be seen in the FITC-SYBR Green I and overlay images of the nucleus isolated using the Celegans protocol in **Figure 1 E;** the arrow (ii) points to a broken nuclear membrane is shown leaking fluorescently stained nucleic acid contents. In contrast, most nuclei isolated from the Frankenstein protocol have smooth and intact membranes, and various nuclei sizes were recovered (iii), suggesting the recovery of nuclei from diverse cell types.

In summary, the Frankenstein protocol generated the most RNA per nucleus and the most consistent morphologically robust and diverse nuclei, despite slightly lower total nuclei recovered than the HCA protocol.

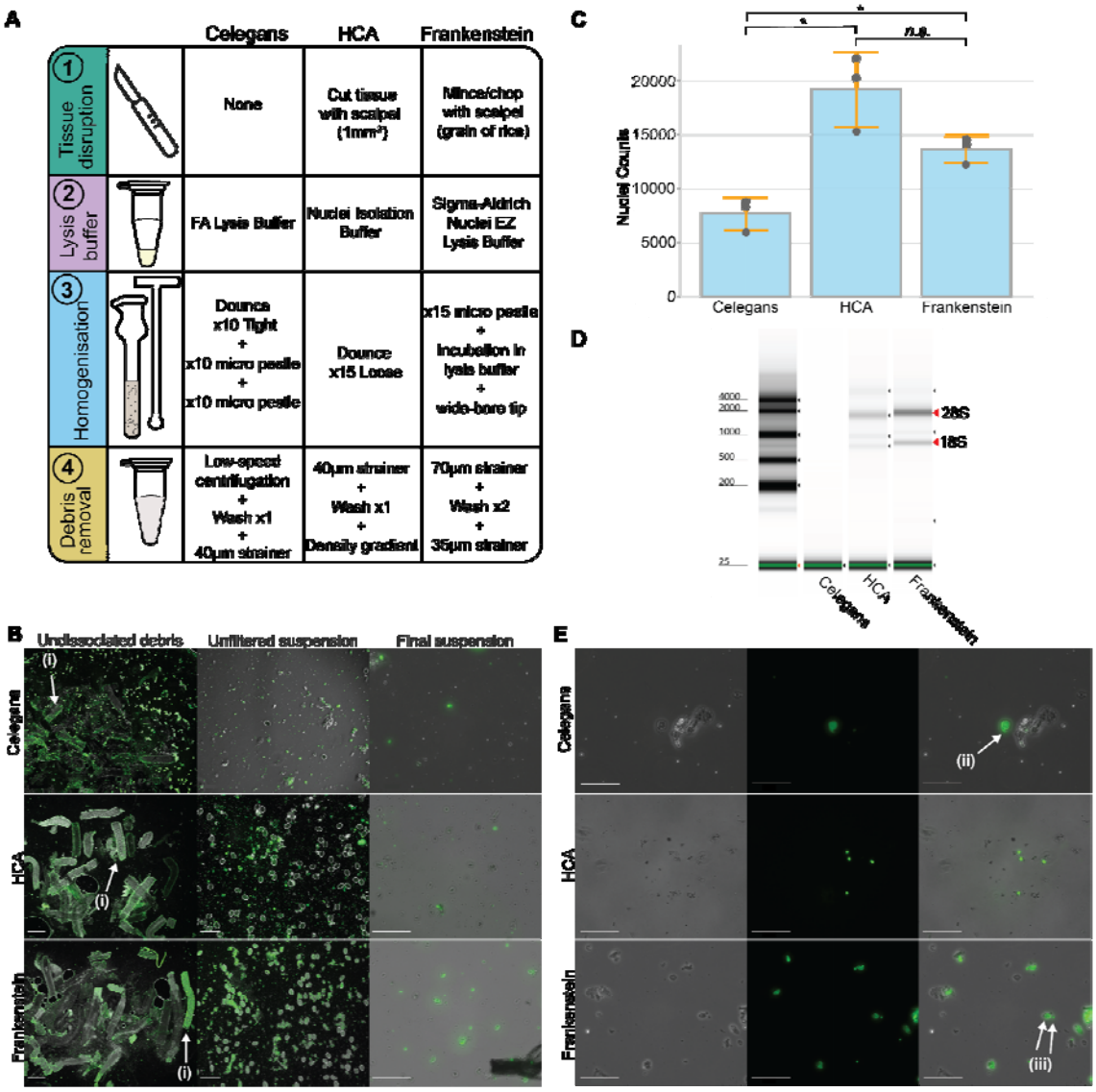

Figure 1. Nuclei isolation of adult female *Haemonchus contortus* worms using three representative protocols. A) Schematic comparison of the three nuclei isolation methods. B) Representative images from the Celegans, HCA, and Frankenstein protocols of the undissociated debris remaining after homogenisation (i), unfiltered suspension, and final washed nuclei suspensions. Images are overlays of phase contrast and fluorescent microscopy of SYBR Green I-stained samples. Scale bars = 500, 250, and 50 µm for "Undissociated debris", "Unfiltered suspension", and "Final suspension", respectively. C) Manual nuclei counts from each protocol. Error bars represent the standard deviation of the mean of three replicates. The asterisk (*) denotes statistical significance between nuclei counts (p = 0.0065). D) Representative Agilent HS RNA Tapestation gel of RNA extracted from nuclei suspensions from each protocol. E) Representative phase contrast and SYBR Green I stained fluorescent images of the final nuclei suspensions. Scale bars = 50 µm. The white arrow points denoted with (ii) point to a broken nuclear membrane that is shown

leaking fluorescently stained nucleic acid contents. In contrast, most nuclei isolated from the Frankenstein protocol have smooth and intact membranes, and various nuclei sizes were recovered (ii), suggesting the recovery of nuclei from diverse cell types.

Optimisation of the **S**ingle **N**uclei Isolation of **P**arasites (**SNIP**) protocol

Next, we sought to improve nuclei isolation in parasitic nematodes based on lessons learned from performing the three initial protocols. The key stages of the optimised protocol are outlined in **Figure 2 A** and summarised in **Table 1**.

We used frozen worms, which enabled greater flexibility in collecting and storing samples before processing. However, one disadvantage of the HCA and Frankenstein protocols was that the tissue was minced or chopped with a scalpel in a petri dish on wet ice, resulting in the worms immediately thawing, which could lead to degraded RNA and decreased nuclei quality if not processed quickly. To prevent this, for the macroscopic stages (e.g. adult worms of *H. contortus* and *T. muris*), we used spring scissors to cut through the cuticle and obtain <2 mm pieces in the sample tube on dry ice. We then ground the microscopic stages (e.g. larvae of *H. contortus*) using a mortar and pestle placed in dry ice. This technique enabled the tissue to be kept in a single tube and minimised sample loss, which is important when the starting material is limited while keeping the sample frozen.

Damaged nuclei release soluble, “sticky” DNA, which can result in the clumping of intact nuclei. To address this, we included a DNase I enzyme and required $MgCl_2$ in the lysis buffer. Similarly, when lysing cells for single nuclei isolation, RNases are released; thus, to prevent RNA degradation, we added an RNase inhibitor to both the lysis and wash buffers. We note that several RNase inhibitors are commercially available; however, some brands have been associated with lower cDNA yields when used for specific scRNA-seq protocols and technologies [23]. Therefore, we suggest selecting a recommended RNase inhibitor based on the intended downstream single-cell platform.

The Frankenstein and HCA protocols resulted in a large amount of undigested tissue, whereas homogenisation in the Celegans protocol was too harsh (**Figure 1 B**). Therefore, we optimised the Dounce homogenisation, focusing on the number of strokes and using different-sized Dounce tissue grinder pestles. We found that five strokes with the loose Dounce tissue grinder pestle exposed worm tissue that had not been adequately disrupted with scissors in the previous step, and released the first nuclei from well-exposed tissue

pieces. Then, using the tight Dounce tissue grinder pestle, tissue and cells were lysed to release the maximum number of nuclei. After each set of strokes with the Dounce tissue grinder pestles, the large undigested tissue pieces were allowed to settle for up to 4 minutes, and the suspended nuclei in the supernatant were collected to prevent lysis from further homogenisation. This additional short incubation in the lysis buffer allowed the complete lysis of the cells within larger chunks of worm tissue. Collecting the nuclei suspension throughout the homogenisation is a step taken from the Celegans protocol. Homogenisation was deemed complete when the suspension was clear to the naked eye.

Removing both small and large debris in nematode nuclei suspensions is necessary due to the amount of debris generated from the cuticle and lysed cells; however, each method and iteration of debris removal results in nuclei loss and additional processing time. We found that large debris was best removed by allowing the debris to settle by gravity during dissociation and filtering the final suspension through a 30 µm cell strainer. To ensure maximal recovery and minimise nuclei loss, we washed the cell strainer with additional wash buffer and pipetted the suspension through on the side of the filter with the tip against the mesh. However, we found the only effective and efficient way to remove small debris from the nuclei suspensions was through Fluorescence-Activated Cell Sorting (FACS). Small cellular and cuticle debris, abundant in the pre-sorted female *H. contortus* sample (**Figure 2 B**), are removed efficiently with FACS (**Figure 2 C**). The gating strategy for selecting SYBR Green I positively stained nuclei for FACS was determined using an unstained negative control (**Supplementary Figure 1)**.

We compared the nuclei count and RNA quality of our optimised nuclei isolation protocol with those of the three tested protocols. When starting with the same amount of adult worms, the optimised protocol had a mean recovery of 31,797 nuclei, amounting to 4.1-fold more nuclei than the Celegans protocol ($p = 0.0001$, $t(4) = 18.8851$), 1.7-fold more than the HCA protocol ($p = 0.0049$, $t(4) = 5.6394$), and 2.3-fold more nuclei than the Frankenstein protocol ($p = 0.0001$, $t(4) = 15.4725$). The RNA concentration for the optimised protocol was 210.0 ng, which equated to approximately 2.62 pg/nucleus; this represented a 3.23-fold increase in RNA received per nucleus relative to 0.81 pg/nucleus from the previous best-performing Frankenstein protocol. The resulting nuclei have smooth nuclear membranes, and very few nuclei showed signs of damage (**Figure 2 B, C**), indicating a high-quality suspension to proceed with sequencing library preparation.

Table 1. Critical steps in protocol optimisation

Protocol step	Modification	Description
Tissue disruption	Cut frozen worms in the sample tube on dry ice using spring scissors	Cutting worms with scissors on dry ice exposes internal tissues for lysis and reduces RNA degradation, loss of sample and balanced homogenisation
Lysis	Sigma-Aldrich Nuclei EZ Lysis Buffer*, with the addition of 0.2 U/µL RNase Inhibitor, 25 µg DNase I, 5 mM $MgCl_2$	DNase I digests any "sticky" free DNA from nuclei that lyse, preventing clumping; $MgCl_2$ is required for DNase I activity and stabilises chromatin; RNase Inhibitor protects RNA in nuclei from degradation by RNases released during tissue/cell lysis
Homogenisation	1 mL Wheaton Dounce tissue grinder 5x loose pestle, 3x tight pestle (repeat 3x tight pestle up to 3x)	Glass Dounce tissue grinder resulted in better homogenisation of the worms than plastic pestles
	Each douncing set is followed by a 2 min incubation on ice to allow large undissociated worm fragments to settle, and nuclei in suspension are collected	Collecting nuclei after each Dounce homogenisation set eliminates the risk of over-douncing and lysing nuclei. Incubating the suspension on ice after each Dounce homogenisation set maximises the effectiveness of the lysis buffer.
Debris removal	1x wash using 2% BSA-PBS with 0.2 U/µL RNase Inhibitor and 5 mM EDTA	Only one wash, using a higher percentage of BSA with RNase Inhibitor added, is performed to minimise the loss of nuclei. Pre-filtering the homogenate through a 70 µm strainer is not necessary when collecting the homogenate after each Dounce homogenisation set because the large debris remains settled in the bottom of the Dounce tube.
	30 µm CellTrics filter, then FACS	A 30 µm strainer removes nematode eggs; washing the CellTrics filter after filtering the homogenate increases the recovery of nuclei
Miscellaneous	Low-binding pipette tips and tubes	Low-binding tips can increase recovery; they can be BSA-blocked for increased recovery
	5 mL Eppendorf Protein LoBind tubes	Increased recovery is observed with LoBind tubes that can fit in a 15 mL adapter in a swing-bucket rotor; they can be BSA-blocked for increased recovery
	Swing-bucket benchtop centrifuge	Swing-bucket rotor pellets nuclei at the bottom of the tubes and results in a lower likelihood of disturbing the pellet during washes

*0.32 M sucrose; 5 mM $CaCl_2$; 3 mM magnesium acetate; 0.1 mM EDTA; 10 mM Tris, pH 8.0

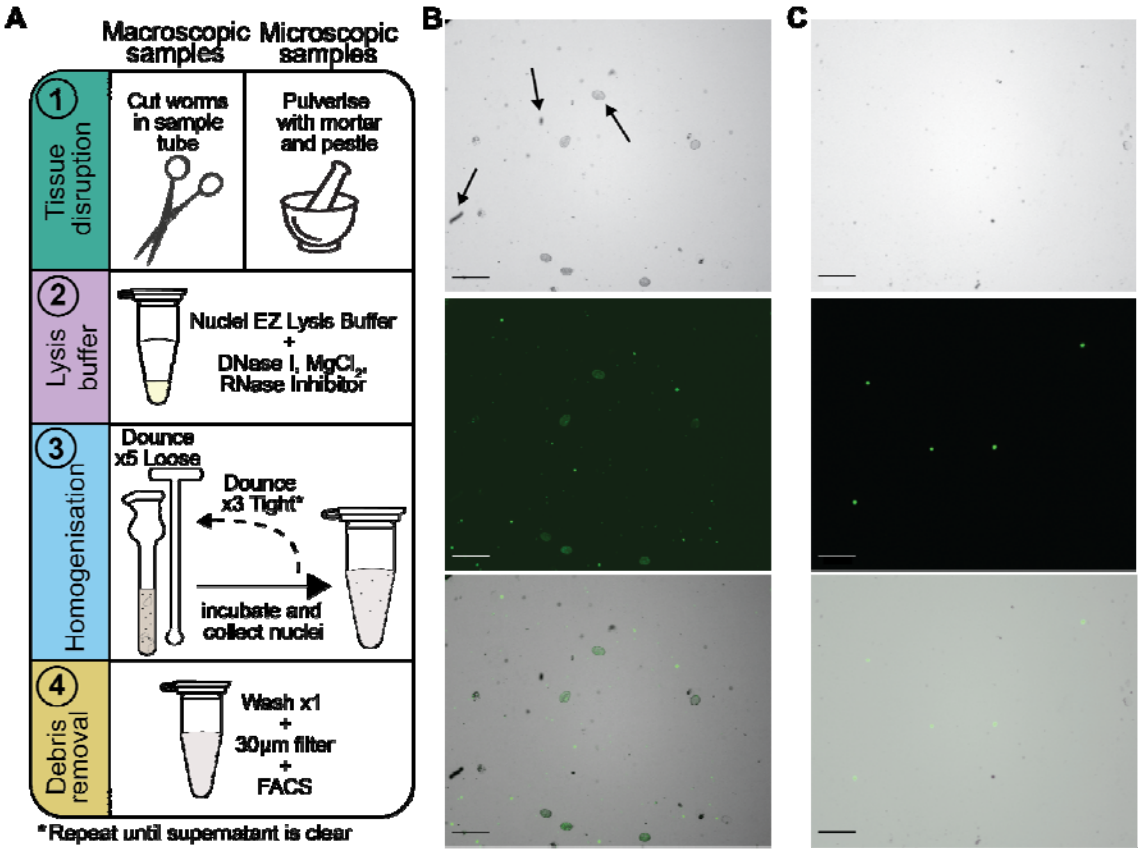

Figure 2. Overview of the Single **N**uclei Isolation of **P**arasites (**SNIP**) **protocol.** A) Schematic comparison of the optimised SNIP protocol for macroscopic (adult worms) and microscopic (eggs and larvae) samples; B) Representative phase contrast, SYBR Green I stained fluorescent, and overlay images of nuclei after washing and filtering. Arrows indicate debris, for example, eggs and cuticle pieces. Scale bar = 100 µm; C) Representative images of the *H. contortus* adult female nuclei suspension after debris removal by FACS. Scale bar = 100 µm.

Validation of the SNIP protocol on multiple life stages of *H. contortus and T. muris*

Once optimised, we further tested our protocol with adult male, adult female, and third-stage (L3) larvae of *H. contortus* and with adult female and male *T. muris* (mouse whipworm), a biologically and phylogenetically distinct parasitic nematode species [24].

The microscopic size of L3 larvae of *H. contortus* precludes the use of scissors to cut the cuticle of the worms in the tissue disruption step of our protocol. Therefore, to ensure tissue disruption of this life stage, we ground the frozen larval pellet using a porcelain mortar and pestle on dry ice and then transferred the sample to the Dounce tube using a microspatula.

Next, we optimised the number of sets of Dounce homogenisation strokes with the tight Dounce tissue grinder pestle. Homogenisation of the macroscopic adult worm samples was completed after one set of the loose Dounce tissue grinder strokes and two sets of tight Dounce tissue grinder strokes, as evidenced by a clear supernatant in the Dounce tube. In contrast, L3 larvae did not homogenise as easily and required additional sets of homogenisation with the tight Dounce tissue grinder pestle until the supernatant in the Dounce tube was clear to the naked eye. This was validated by fluorescent staining of aliquots of the supernatant after each round. In our hands, a maximum tissue volume equivalent to 20 µL per 1 mL Dounce capacity was optimal without requiring excessive time to complete homogenisation. Importantly, additional sets of the tight Dounce tissue grinder strokes do not result in nuclei lysis because the supernatant containing nuclei is collected after each Dounce homogenisation set.

Manual nuclei counts for three independent replicates of each species and life stage tested are shown in **Figure 3 A**. For *H. contortus*, ten adult females, 20 adult males, and ~250,000 microscopic L3 larvae were used per replicate (n = 3), which was approximately the same volume per tube. For *T. muris*, 25 adult female and 25 male parasites were included per replicate (n = 3). Although our protocol was optimised using female *H. contortus,* it proved even more effective on the female *T. muris* samples; the number of nuclei isolated per worm was significantly higher in the adult female *T. muris* ($\bar{x}$ = 26,675.33 nuclei/worm) than in *H. contortus* ($\bar{x}$ = 3,570 nuclei/worm) (p = 0.0001, t(4) = 15.9198). This is, in part, explained by the differences in parasite size; adult female *H. contortus* worms are between 20-30 mm x 300-500 µm, and adult female *T. muris* worms are 35-50 mm x 40-600 µm (**Figure 3 B**). The large range in width of *T. muris* is due to its whip-like intracellular anterior end. RNA recovery was 210.0 ng for *H. contortus* females, 37.9 pg for *H. contortus* males, 23.9 ng for *H. contortus* L3s, 901.6 ng for *T. muris* females, and 2,310.0 ng for *T. muris* males. This equates to approximately 2.62 pg/nucleus for *H. contortus* females, 0.53 pg/nucleus for *H. contortus* males, 0.17 pg/nucleus for *H. contortus* L3s, 1.66 pg/nucleus for *T. muris* females, and 2.50 pg/nucleus for *T. muris* males.

The FACS analysis of samples collected and fixed for snRNA-seq is shown in **Figure 3 C**. Nuclei were sorted on a SYBR Green I positive signal (shown in the green box) with percentages of total events presented (**Figure 3 C**). An aliquot of unstained nuclei was used to determine gating for a SYBR Green I positive signal (FACS plots shown in **Supplementary Figures 1-2**). The distinct clusters of SYBR Green I fluorescence-positive nuclei in the adult worm samples reflect different levels of ploidy within nuclei populations

that, while well understood in the free-living model nematode *C. elegans* [25], are observed here for the first time for *H.contortus* and *T. muris.*

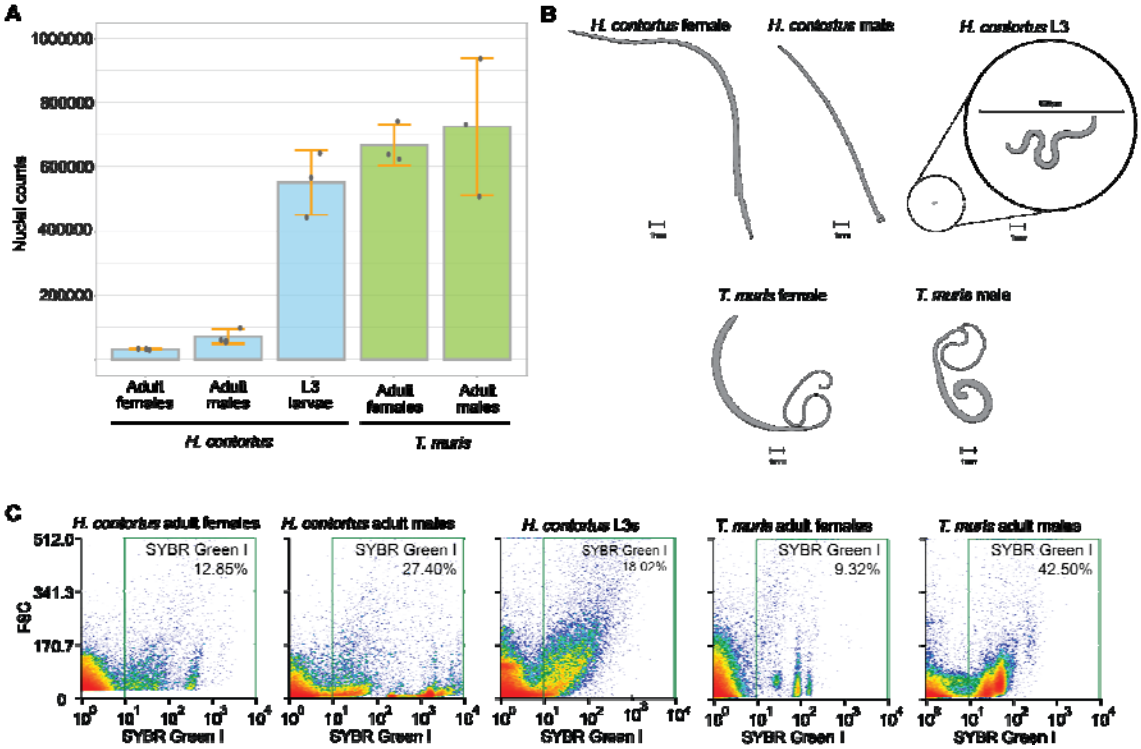

Figure 3. Comparison of the Single Nuclei Isolation of Parasites (SNIP) protocol on different species and life stages. A) Nuclei counts of each species and stage using the SNIP protocol. For *H. contortus*, ten adult females, 20 adult males, and ~250,000 microscopic L3 larvae were used per replicate (n = 3), which was approximately the same volume per tube. For *T. muris*, 25 adult female and 25 male parasites were included per replicate (n = 3). B) Representative outlines of *H. contortus* and *T. muris* worms used in the study, highlighting the relative differences in size between life stages and species. C) Representative Fluorescence-Activated Cell Sorting (FACS) plots of each species and stage tested using the optimised nuclei isolation protocol. Gating for a positive SYBR Green I signal was determined based on an unstained negative control nuclei aliquot from each sample (shown in **Supplementary Figure 2**). The x-axis displays SYBR Green I fluorescence in log scale using the 488 nm laser and 507/19 filter. The y-axis is the forward scatter area (FSC-A) on a linear scale.

Single-nuclei RNA sequencing identifies distinct cellular populations in different parasite life stages

To validate our optimised nuclei isolation protocol, we performed snRNA-seq on the nuclei suspensions obtained from the different species and life stages. We chose to use the Parse Biosciences Evercode platform, based on Split Pool Ligation-based Transcriptome

sequencing (SPLiT-seq) [26], over other commercial high-throughput platforms, such as 10x Genomics Chromium, to enable greater flexibility in sampling different life stages throughout a life cycle (in preparation for developmental cell atlases). Specifically, with this technology, nuclei preparations from individual stages could be collected at different times, fixed, and stored frozen for up to six months before library preparation, enabling the processing of different samples together and thus minimising a source of technical bias between samples and replicates. Parse is not the only option to fix and store samples before processing. For example, Roux et al.[27] used methanol-fixed cells from *C. elegans* with the 10x Chromium Single Cell 3' Chemistry, however, but a minimum of 3-4 million cells was required (significant higher than proposed here), and nuclei were not tested. We also considered the ability to pool up to 384 samples in a single experiment when scaling up, the ability to better detect lowly expressed genes and avoid ambient RNA common in droplet-based techniques, and that no specialised equipment is required. Additionally, the Parse Biosciences Evercode platform uses both poly(A) and random primers to capture mRNA, enabling broad gene coverage and the detection of non-coding RNAs[26].

We performed two rounds of library preparation and sequencing, designated "experiment 1" and "experiment 2," using the Parse Biosciences Evercode WT Mini kit. This kit enables the sequencing of up to 10,000 nuclei, distributed across 1 to 12 samples, per experiment. **Table 2** shows the total nuclei and median genes and transcripts per nucleus from sequencing nuclei libraries of the two parasites and different life stages from experiments 1 and 2. In experiment 1, we obtained consistent counts of genes and transcripts per nuclei for all stages. However, the total nuclei counts were more variable, with higher counts for *T. muris* adult females (n = 1,291) and lowest for *H. contortus* adult males (n = 216). For experiment 2, we increased the number of starting nuclei, which increased the number of total nuclei recovered. Further information about input for Parse Evercode WT Mini kit barcoding and sequencing statistics can be found in **Supplementary Table 1.**

To investigate the potential differences between experiments 1 and 2, we further analysed the *H. contortus* samples from experiments 1 and 2 (**Supplementary Figure 4**). The number of genes per nucleus from each sample group is consistently high across all clusters except for Cluster 0, which is dominated by nuclei from Experiment 2, L3 larvae **(Supplementary Figure 4 A-B).** All samples contribute nuclei to every cluster **(Supplementary Figure 4 A, C-G)**. Still, the proportion of nuclei contributing to each cluster varies, as expected, because the experiments were not designed to capture all cell types and the targeted number of nuclei sequenced from each sample is relatively small, compared to a comprehensive cell

atlas. Overall, we do not see a clear difference in clusters of nuclei between the two experiments.

The sequencing aimed to validate the library preparation approach on various sample inputs, not to generate comprehensive scRNA-seq data for a full description of transcriptional variation, which requires far larger numbers of nuclei or cells per sample. Nonetheless, despite low sample input, analysis of transcript expression per species revealed clusters of nuclei based on: 1) life stage and sex (**Figure 4 A,F** for *H. contortus* and *T. muris*, respectively); and 2) clustering of nuclei that were shared or unique to life stages and cell and tissue-specific variation and differentiation (**Figure 4 B,G**). Here, we have inferred the putative function of each cluster based on gene set enrichment and orthology from the model free-living nematode *C. elegans*, revealing stage and tissue-specific gene expression such as putative mechanosensory neurons in *H. contortus* L3 (**Figure 4 C**) and vulval muscle (**Figure 4 D**) and sensory neurons (**Figure 4 E**) specific to adult female and males, respectively. Similar stage and tissue-specific expression were observed in *T. muris*, highlighting nuclei associated with gametogenesis (**Figure 4 H**) and highly distinct neurons (**Figure 4 I**) specific to males, as well as a cluster highly enriched in WAP-domain/S1 peptidase protein expression-specific to females (**Figure 4 J**). We acknowledge that significant evolutionary and phylogenetic differences between *C. elegans* and the parasite species examined here mean that “marker genes” used to characterise a cell or tissue type must be applied cautiously. Considering the sparse functional annotation information for non-model species such as parasitic nematodes [28], data such as these represent both a challenge and an opportunity for improving genomic resources for these species and toward building more comprehensive cell and nuclei atlases for understanding their biology.

Table 2: Comparison of nuclei sequencing of different species and life stages from two experiments

		Experiment 1				Experiment 2			
Species	**Stage**	**Nuclei**	**Genes/ nucleus***	**Transcripts/ nucleus***	**Reads/ nucleus****	**Nuclei**	**Genes/ nucleus**	**Transcripts/ nucleus**	**Reads/ nucleus****
H. contortus	**Adult male**	216	337	589	46,998	868	1,379	4,073	33,850
	Adult female	522	436	714	57,900	7,405	910	2,239	24,864
	L3	647	370	535	93,473	3,606	44	48	3,984
T. muris	**Adult**	614	392	646	137,474	342	105	137.5	115,703

	male								
	Adult female	1,291	295	567	91,630	1,711	71	116	8,186

*The number of genes and transcripts per nucleus reflect median values.

**The number of reads per nucleus reflect mean values

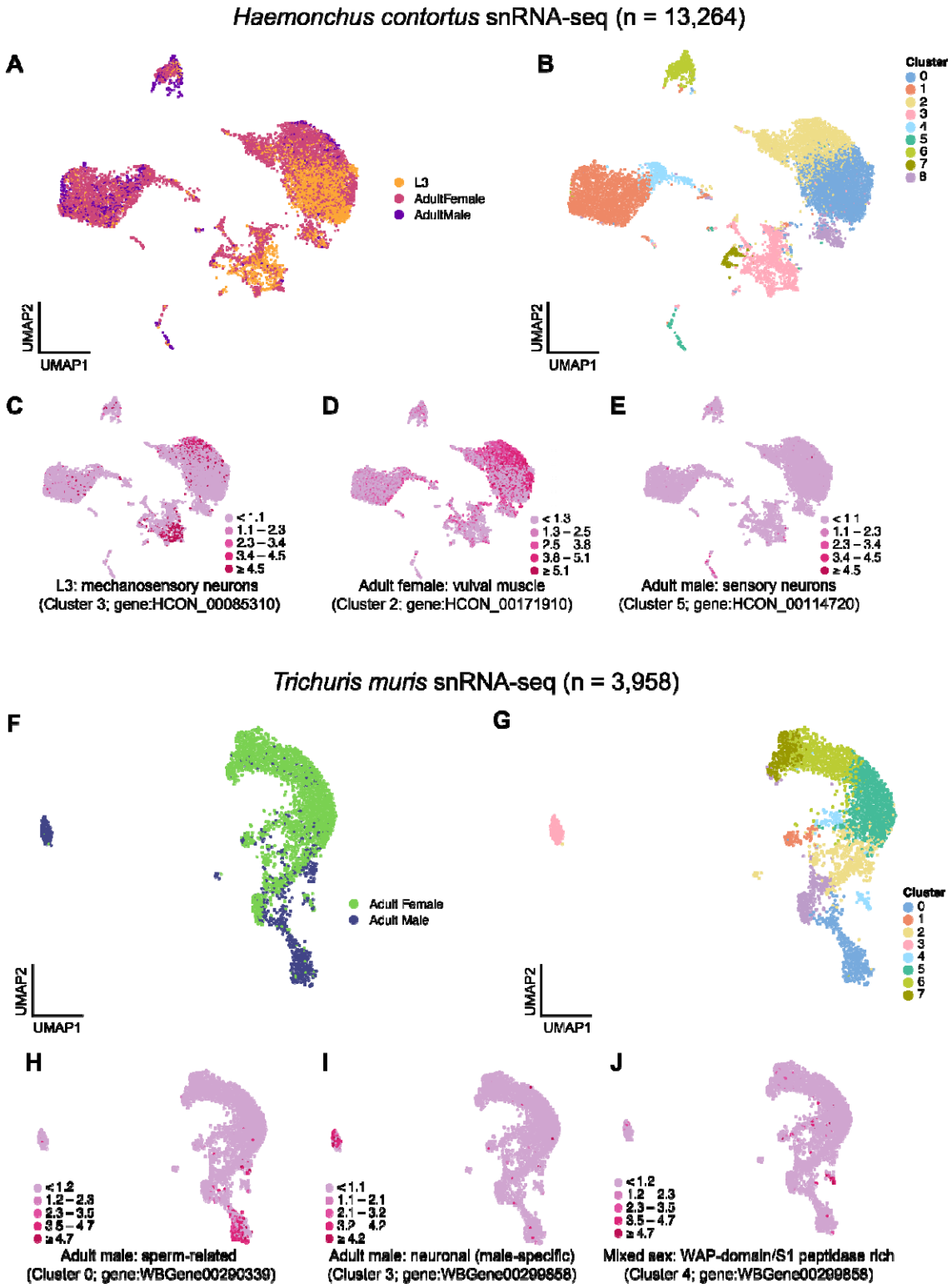

Figure 4: Single-nuclei RNA sequencing of different life stages of *Haemonchus contortus* and *Trichuris muris.* Uniform Manifold Approximation and Projections (UMAPs) of snRNA-seq data from (A-E) *H. contortus* (n = 13,264 nuclei) and (F-J) *T. muris* (n = 3,985 nuclei) coloured by (A, F) life stage or nuclei cluster (B, G). In total, 8 nuclei clusters were

predicted from three life stages (adult male, adult female, L3) of *H. contortus*, and 7 nuclei clusters from two life stages (adult male, adult female) of *T. muris*. In C-E and H-J, we highlight three examples of biologically meaningful clusters from both datasets, demonstrating sex and stage-specific gene expression (colour scale: log normalised expression counts) with inferred functional roles based on *Caenorhabditis elegans* orthology and gene set enrichment from the top 20 differentially expressed genes per cluster.

Discussion

In this study, we evaluated three existing protocols for isolating single nuclei for snRNA-seq, from which we optimised a method for recovering nuclei from parasitic nematodes (SNIP). Our motivation for this work is to create robust cell atlases that will enhance our understanding of parasitic nematode development, illuminate the tissues and organs that mediate interactions with their hosts, and identify novel drug targets and mechanisms of drug resistance. Here, we discuss the rationale of our approach, challenges faced, and ongoing limitations to be overcome towards applying snRNA-seq for parasitic nematodes specifically, but more generally, the application of cellular-resolution technologies toward other complex and enigmatic non-model organisms.

The use of single-cell and single-nuclei RNA sequencing to understand the fundamental biology of organisms at cellular resolution is advancing rapidly. Although there are successful examples of cell atlases of specific life stages or tissues of multicellular parasites using scRNA-seq [8–14,16], we specifically chose to use snRNA-seq for several reasons. First, we aim to collect and analyse different life stages of parasites over time and in response to perturbations, such as drug treatment exposure. Whereas scRNA-seq typically requires the rapid processing of fresh tissue and live cells after recovery through to library preparation, snRNA-seq enables sample preservation via freezing, allowing the collection of samples over time that can be processed together, thus reducing library and sequencing batch effects. Here, we demonstrated the versatility of the protocol by sampling multiple species and life stages, each derived from different hosts (*H. contortus* in sheep and *T. muris* from mice) and sampling strategies (invasive and non-invasive sampling from hosts). Moreover, the freezing of parasites enabled sample collection and shipment from geographically distant collaborators rather than having to be physically located with the specimens at the time of collection for immediate processing. Such an approach opens up the possibility of sampling other non-model organisms from diverse or difficult-to-access locations worldwide, provided they can be frozen shortly after collection. The second reason for a nuclei-focused approach is the challenge of tissue dissociation into living cells. Both scRNA-seq and snRNA-seq aim to mirror the transcriptome of cells in tissue, and thus, the recovery of "healthy" cells is paramount. However, stress caused by a combination of physical and/or enzymatic treatment, temperature, and time can alter transcriptional profiles and result in artefacts during data analysis [29,30]. Therefore, effective cellular disassociation of an organism or tissue for scRNA-seq requires a balance between sufficient effort (physical or enzymatic) to disassociate and sufficient care not to damage cells or nuclei so they can be processed. The dissociation of frozen tissue to collect nuclei, in which transcriptional profiles are less

susceptible to change and therefore better reflect the transcriptome signature of the cells, can be preferred for difficult-to-dissociate tissues that require greater physical forces to be applied during disassociation. We anticipated this to be important for dissociating parasitic nematodes, many of which are protected by a strong acellular cuticle and sheath and can be very resistant to breaking. Furthermore, our optimised protocol significantly improved the disassociation time; the original protocols tested took ~40-45 minutes to complete, whereas the optimised protocol took ~25 minutes. Other advantages of snRNA-seq over scRNA-seq include the capture of a greater diversity of cell types [31], likely due to differential susceptibility to damage between cell types, and the physical constraints of cell size of commonly used microfluidic technologies, for example, 10x Genomics has a recommended maximum cell size limit of 30 µm and a maximum physical microfluidic channel width of 50-60 µm. Cell sizes are known to vary significantly in nematodes; for example, during the development of the model free-living nematode *C. elegans*, the intestine significantly increases in tissue volume through to adulthood primarily due to intestinal cells growing in size, becoming multinucleated and polyploid, rather than a large increase in cell number by cell division [25]. We anticipate similar cell-size variation in the closely related *H. contortus* and may also apply to specialised tissues such as the elongated stichosome of *T. muris* [32]. Moreover, approximately 30% of *C. elegans* somatic nuclei are contained in large, multinucleated cells due to cellular fusion during development to form complex tissues [33]. Due to their unusual cell morphology properties, these cell types are likely to be better represented in snRNA-seq data than in scRNA-seq data.

We overcame several challenges during protocol development. For adult stages of parasitic worms, we found that chopping frozen tissue in a single tube on dry ice resulted in more efficient disassociation and lysis than thawing and mincing tissue. However, dissociating microscopic *H. contortus* L3 larvae, an environmentally robust free-living life stage with a sheath surrounding its external cuticle [34], proved more challenging. We explored several approaches, including a *C. elegans* nuclei isolation protocol by Cao *et al.* [35] that used shearing forces from pipetting samples through a 21 G needle for initial tissue disruption. However, in our hands, the *H. contortus* L3 larvae did not shear, whereas the larger adult stages persistently clogged the needle. Our approach of pre-grinding frozen L3 with a porcelain mortar and pestle, followed by a combination of loose and tight Douce strokes and recovery of nuclei in between sets of strokes, improved nuclei recovery significantly. Throughout the protocol, nuclei were lost at each step. We tackled this by recovering nuclei during homogenisation in stages, which prevented excessive mechanical damage and thus maximised the collection of intact nuclei. Once collected, nuclei needed to undergo filtration to remove large and small debris; we found that a single wash step and a 30 µm filter with a

filter wash removes sufficient small and large debris to prevent clogging of the FACS machine capillaries while minimising nuclei loss. The Celegans protocol recommended using Flowmi Cell Strainers, which attach directly to a pipette; however, we found they were easily clogged by the amount of debris in parasitic nematode nuclei suspensions and could not be easily washed to increase nuclei recovery. Furthermore, while FACS removes small debris, reveals diverse nuclei populations, and provides another count measurement, it can also lead to loss of nuclei and decreased nuclei quality [36]. The use of FACS as a filtration step may depend on the degree of debris, and may be worth comparing nuclei for sequencing with and without FACS if debris is minimal. We also experienced nuclei loss during the fixation process of the Parse Biosciences Evercode protocol for snRNA-seq. Parse Biosciences recommends that high nuclei numbers be fixed to account for loss [37]; however, the loss seems sample-dependent and fixation requires optimisation to minimise its impact. For example, the *T. muris* adult male nuclei suspension had a 69.33% nuclei loss vs only 11.88% for *T. muris* adult female samples. This result suggests that some nuclei are more fragile or could be indicative of more extensive nuclear blebbing in the *T. muris* male nuclei, causing an already compromised nuclear envelope to lyse during fixation [38]. Similarly, the Parse Biosciences WT Mini library preparation requires high sample inputs (~55,000 cells/nuclei) at particular concentrations (between 298 and 3,575 cells/nuclei per µL as determined by the number of samples), which can be challenging to achieve with low biomass samples. One potential solution is to combine and concentrate fixed nuclei samples to obtain the proper input concentration, with the caveat that it can result in significant overall nuclei loss due to additional centrifugation and resuspension.

We acknowledge several limitations to our study. While we have gained insights from the two specific parasitic nematode species tested, nuclei isolations from other species (and extension to other non-model organisms) may present their own challenges and require species-specific optimisation, specifically in regard to the number of Dounce tissue grinder strokes. Some variation in nuclei counts may be due to differences in the susceptibility or resistance of some tissues and cell types to disruption. Until more dense atlases are created and a better understanding of cellular/nuclei proportions is made, this is difficult to address. We used Parse Biosciences for library preparation to enable the storage and simultaneous processing of different samples across life stages. However, as described above, the fixation and thawing lead to considerable nuclei loss. If individual or few samples can be processed without freezing and thawing after fixation, higher nuclei counts and more input material for library prep will likely be achieved.

Conclusions

We have built on existing approaches to develop an optimised protocol for single nuclei isolation of parasitic nematodes for snRNA-seq. Validation on several diverse species and multiple life stages demonstrates versatility, and critical evaluation of crucial steps enables a significant head-start for using this protocol to isolate nuclei from other non-model organisms. The increasing accessibility of cellular-resolution techniques and optimised protocols will advance the understanding of organisms, such as parasitic nematodes, from fundamental biology to infection and disease, and toward novel approaches to control them.

Materials and Methods

Trichuris muris

Mice

NSG (NOD.Cg-*Prkdc*^{scid} *Il2rg*^{tm1Wjl}/SzJ) mice were maintained under specific pathogen-free conditions, under a 12 h light/dark cycle at a temperature of 19-24°C and humidity between 40 and 65%. Mice were fed a regular autoclaved chow diet (LabDiet) and had *ad libitum* access to food and water. All efforts were made to minimise suffering through considerate housing and husbandry. Animal welfare was assessed routinely for all mice involved. Mice were naive before the studies described here.

Experiments were performed under the regulation of the UK Animals Scientific Procedures Act 1986 under the Project license P77E8A062 and were approved by the Wellcome Sanger Institute Animal Welfare and Ethical Review Body.

Infection and egg collection

Infection and maintenance of *T. muris* were conducted as described [39]. Briefly, NSG mice (6-8 weeks old) were orally infected under anaesthesia with isoflurane with a high dose of embryonated eggs (n = 400) from *T. muris* E-isolate. Mice were monitored daily for general condition and weight loss. Thirty-five days later, mice were culled by cervical dislocation and the caecum and proximal colon were removed. The caecum was split and washed in RPMI-1640 supplemented with 500 U/mL penicillin and 500 µg/mL streptomycin (all from Gibco, UK). Worms were removed using fine forceps and cultured for 4 h or overnight in RPMI-1640/penicillin/streptomycin at 37°C, 5% CO_2. The excretory/secretory (E/S) products from the worm culture were centrifuged (720 *g*, 10 min, room temperature (RT)) to pellet the eggs. The eggs were allowed to embryonate for eight weeks in distilled water in the dark at RT [40,41], and infectivity was established by worm burden in NSG mice.

Adult worm collection

Thirty-five days post-infection, mice were culled by cervical dislocation and the caecum and proximal colon were removed. The caecum was split and washed in RPMI-1640/penicillin/streptomycin. Worms were removed using fine forceps, and males and females were sorted into separate 1.5 mL nuclease-free microcentrifuge tubes. All liquid was removed from the worms in the tubes, and the tubes were submerged in liquid nitrogen and stored at -80°C.

Haemonchus contortus

Sheep

Sheep used for experimental infections of *H. contortus* were born and raised under worm free conditions at the Moredun Research Institute, UK. Sheep were humanely euthanased under Schedule 1 of the Animals (Scientific Procedures) Act.

All experimental procedures were examined and approved by the Moredun Research Institute Animal Welfare and Ethics Review Board and were conducted under approved UK Home Office licenses (PPL 60/03899, experimental code identifier E46/11) following the Animals (Scientific Procedures) Act of 1986.

Sheep were infected orally with 5,000 *H. contortus* MHco3(ISE) L3.

Culturing and collection of L3 larvae

Faeces were collected from 21 days post-infection and coprocultured for 14 days to allow development from egg to L3, after which the larvae were recovered using the Baermann technique before storage at approximately 8°C in tap water. To collect the larvae, water containing the larvae was vacuum filtered through a 10 µm cell strainer (pluriSelect 43-50010-03) fitted to a 250 mL filter flask and washed with 50 mL 1x M9 buffer. Larvae were scraped off the cell strainer using a micro spatula (Fisherbrand 11523482), put in a 1.5 mL nuclease-free microcentrifuge tube, immediately submerged in liquid nitrogen, and stored at -80°C.

Adult worm collection

Adult worms were collected from the abomasum of sheep at necropsy 28 days post-infection. Worms were rinsed in physiological saline (0.85% NaCl) and sexed based on morphology, before male and female adults were sorted into separate 1.5 mL nuclease-free microcentrifuge tubes using a needle. The tubes were submerged in liquid nitrogen and stored at -80°C.

Original single nuclei isolation protocols

Frankenstein

The Frankenstein protocol [20] combines strategies of five protocols for nuclei isolation from mammalian brain tissue [42–46]. First, tissue is minced/chopped with a razor blade on wet ice and added to chilled Nuclei EZ Lysis Buffer in a 1.5 mL tube. A plastic pestle is used to

homogenise the sample, and gentle mixing with a wide-bore pipette tip facilitates tissue dissociation. The homogenate is then filtered and washed twice with 1% BSA-PBS. After resuspension in 1% BSA-PBS, the nuclei are filtered through a 35 µm cell strainer and sorted using FACS.

Celegans

The protocol for single-nuclei isolation from the free-living nematode *C. elegans* originates from a publication by Truong et al. [17]. A 30 µL compact pellet of worms is homogenised in FA cell lysis buffer by applying ten strokes of the tight Dounce tissue grinder pestle in a glass Dounce tissue grinder tube. Further homogenisation is performed using ten strokes with a disposable pellet pestle. Homogenisation with the disposable pellet pestle is repeated twice for a total of 20 strokes. After each set of pestle strokes, the supernatant is collected and centrifuged at low speed to pellet large debris. The nuclei in suspension are pelleted, washed with 1% BSA-PBS, and filtered using a 40 µm Flowmi tip filter. Filtered nuclei were sorted using FACS.

Human Cell Atlas (HCA)

The protocol used by the Human Cell Atlas team at the Wellcome Sanger Institute [19] is adapted from the protocol by Nadelmann et al. [47]. The tissue sample is not minced or chopped before placing it in a glass Dounce tissue grinder tube with a homemade homogenisation buffer. A protease inhibitor is recommended to be included in the homogenisation buffer, but we did not include it because it is only necessary for proteomics. The tissue is homogenised with 10-20 strokes using the loose Dounce tissue grinder pestle until no resistance is felt. The tight Dounce tissue grinder pestle is then applied 10-20 times until no resistance is felt. The homogenate is filtered through a 40 µm cell strainer and washed once with 5% BSA-PBS wash buffer. An optional gradient centrifugation step is described using Lymphoprep or Percoll to remove debris.

An optimised protocol for nematode single nuclei isolation

A detailed, step-by-step protocol is available on STAR Protocols. All reagents and equipment are pre-chilled on wet ice unless otherwise stated. Twenty adult female *H. contortus* worms were cut into pieces <2 mm while on dry ice using spring scissors pre-chilled in a 50 mL Falcon tube on dry ice. The tissue is placed in a 1 mL Wheaton Dounce tissue grinder (DWK Life Sciences) containing 500 µL Nuclei EZ Lysis Buffer (Sigma-Aldrich) with the addition of 25 µg/mL DNase I, 5 mM $MgCl_2$, and 0.2 U/µL SUPERase In RNase inhibitor using a glass Dounce tissue grinder. The loose Dounce tissue grinder pestle is applied five times, followed by three strokes of the tight Dounce tissue grinder pestle. The

homogenate is incubated on ice for up to 4 min or until the large undissociated tissue and debris settle. The supernatant containing the nuclei is collected in a 5 mL Protein LoBind tube (Eppendorf). Fresh lysis buffer is added to the Dounce to replace the removed supernatant. Three additional strokes of the tight Dounce tissue grinder pestle are applied, followed by incubation and supernatant collection. Homogenisation with the tight Dounce tissue grinder pestle is repeated up to three more times or until the settled homogenate is clear. The nuclei are pelleted, washed once with 2% BSA-PBS wash buffer containing 0.2 U/µL SUPERase·In (ThermoFisher) and 5 mM EDTA, and filtered using a 30 µm CellTrics filter (Sysmex). Nuclei isolation should take no more than 30 min. The filter is washed with additional wash buffer to maximise the recovery of nuclei. Nuclei are sorted using FACS to remove small debris.

Flow cytometry and Fluorescence-Activated Cell Sorting (FACS)

The Bigfoot Spectral Cell Sorter (ThermoFisher) was used to assess and sort nuclei. A 50 µL aliquot of nuclei from each sample was used as a negative control for fluorescent staining detection levels. The remaining sample (~500 µL) was stained with 5 µL 1,000x SYBR Green I (ThermoFisher) for sorting. Flow cytometry was performed using the 488 nm laser and 507/19 filter. For this study, nuclei were gated only on a positive SYBR Green I signal (**Figure 3C, Supplementary Figure 2**) to avoid omitting the unusually small and large nuclei observed in microscopy. Nuclei were collected in pre-chilled 1% BSA-blocked 5 mL Protein LoBind tube (Eppendorf) containing the 2% BSA-PBS wash buffer detailed above and kept on ice.

Sample fixation

After sorting, the nuclei concentration was determined using a C-Chip disposable hemocytometer (NanoEntek). The nuclei suspension was centrifuged for 10 mins at 500 g and 4°C. The Evercode Nuclei Fixation kit (Parse Biosciences) with user manual v2.0.2 was used with the following modifications. The 15 mL polypropylene tubes were replaced with 1% BSA-blocked 5 mL Protein LoBind tubes (Eppendorf). Briefly, tubes were filled with 1% BSA-NFW solution, incubated for 30 mins at room temperature, and then dried in a laminar flow cabinet. All centrifugation steps were done at 500 g. Because our nuclei suspensions were fairly dilute (~100,000 nuclei starting) and nuclei clumping was not observed, we skipped the two 40 µm straining steps in the fixation protocol to maximise nuclei retention. Additionally, due to the low concentration, nuclei were resuspended in only 50 µL of Nuclei Buffer, and the DMSO concentration was adjusted accordingly. Fixed nuclei were placed in a Corning CoolCell Cell Freezing container and stored at -80°C until all nuclei preparations were collected. Fixed nuclei can be stored for up to 6 months.

Library preparation and sequencing

Combinatorial barcoding, cDNA amplification, and library preparation were performed using the Evercode WT Mini v2 kits (Parse Biosciences) and user manual v2.0.1. A 10 µL aliquot of fixed nuclei from each sample's nuclei suspension is thawed at 37°C, and nuclei are manually counted using a C-Chip haemocytometer. Nuclei concentrations are input into the "Parse Biosciences Evercode WT Mini Sample Loading Table V1.2.0", and the amount of sample stock needed is automatically calculated per the user's specific sample number, the desired number of barcoded cells, and the percentage of the library that is represented by each sample. Samples are allocated into specific wells according to the Sample Loading Table. First, sample-specific barcodes are applied to the nuclei, and then reverse transcription takes place. Nuclei from all wells are then pooled and redistributed across a second plate that contains a second barcode. Nuclei are pooled and split on a third plate to add a third barcode. After ligating three total barcodes, nuclei are pooled and counted manually using a C-Chip haemocytometer. Barcoded nuclei can be split into multiple sublibraries according to user needs. We performed seven cycles in the second cDNA amplification step and thirteen cycles in the sublibrary index amplification PCR, according to kit specifications. We performed seven cycles in the second cDNA amplification step and ten cycles in the sublibrary index amplification PCR, as specified by the kit. Nuclei in the sublibraries are then lysed, and a fourth, sublibrary-specific barcode is added by PCR extension. Library preparation adds Illumina-compatible adapters for loading onto a sequencer. The HS D5000 Tapestation assay was used for fragment analysis of the cDNA sublibraries and final libraries for sequencing. The HS dsDNA Qubit assay was used to quantify the sublibraries and final libraries. The cDNA fragment analyses for the sublibraries and final libraries are shown in **Supplementary Figure 3**.

The resulting libraries were combined with 5% PhiX and then each sequenced on an Illumina NovaSeq 6000 lane using 150 bp paired-end reads, generating 316,638,084 and 307,516,986 reads for Library 1 and Library 2, respectively.

Single nuclei RNA-seq analysis

Raw sequencing data were first assessed using FastQC (v0.12.1) (https://www.bioinformatics.babraham.ac.uk/projects/fastqc/) and MultiQC (v1.17) [48] before analysis using the Parse Biosciences split-pipe (v1.1.2) pipeline. Reference genomes and annotations were downloaded from WormBase ParaSite for *H. contortus* (PRJEB506 [49]) and *T. muris* (PRJEB126 [50]). Reference databases for each species were created using *split-*

pipe --mode mkref incorporating both genome (fasta) and annotation (gtf) before raw reads were mapped to each reference database using split-pipe --mode all (parfile: post_min_map_frac 0.01). Trailmaker™ (Parse Biosciences) was used to complete our single cell RNA-sequencing data analysis. Nuclei were first filtered using the default settings of the "Cell size distribution filter" to remove nuclei with low transcript counts using a barcode rank plot per sample. The default third-order spline model was applied to the data using the "Number of genes vs transcripts filter" to remove outlier nuclei with too few or too many genes vs transcripts. Finally, "Doublet filter", which uses the scDblFinder[51] algorithm, was used to filter out nuclei with a high probability of being a doublet. Mapping statistics, including reads mapped, nuclei identified, and the number of genes and transcripts per nuclei, were collated and visualised from the resulting HTML reports.

Further analysis, including nuclei cluster identification based on differentially expressed transcripts, generation of UMAP plots, and exploration of cluster identity based on marker genes, was performed in Trailmaker™ (Parse Biosciences). UMAPs were visualised, combining all life stages per species and subsequently coloured by life stage or cluster ID. Expression of select genes to highlight cluster specificity and identity was visualised in Trailmaker™ (Parse Biosciences). To infer the biological relevance or putative tissue type of each cluster, the top 20 differentially expressed genes per cluster were obtained, from which the *C. elegans* orthologs were identified using WormBase ParaSite Biomart [52]. Functional enrichment was performed using the *C. elegans* orthologs and the web platform WormEnrichr [53,54]. The parasite genes were also assessed using species-specific GO terms using g:Profiler (version e111_eg58_p18_f463989d) [55].

Code and data availability

Reference genomes and annotations used in the analysis can be accessed from WormBase ParaSite (https://parasite.wormbase.org/). Raw sequencing data can be accessed from the European Nucleotide Archive (ENA) under the study accession ERP140984. The code used to analyse sequencing data can be accessed from https://github.com/stephenrdoyle/single_cell_optimisation. Any additional information required to reanalyse the data reported in this paper is available from one of the lead contacts.

Acknowledgements

We gratefully acknowledge the technical support and advice of Ian Pittam from Parse Biosciences, the Pathogen Informatics group at the Wellcome Sanger Institute for informatics support, and the Helminth Genomics group at the Wellcome Sanger Institute for constructive feedback on the analyses and manuscript.

This work is supported by a UKRI Future Leaders Fellowship to SRD [MR/T020733/1] and the Wellcome Trust (UK) through core funding to the Wellcome Sanger Institute (UK) [206194]. AAM and DJB receive underpinning national capacity funding from the Rural and Environment Science and Analytical Services (RESAS) division of the Scottish Government. M.A.D-C was supported by the Sir Henry Dale Fellowship jointly funded by the Wellcome Trust and the Royal Society (222546/Z/21/Z); the Wellcome Trust (203151/Z/16/Z, 203151/A/16/Z) and the UKRI Medical Research Council (MC_PC_17230). For the purpose of Open Access, the author has applied a CC BY public copyright licence to any Author Accepted Manuscript version arising from this submission.

References

1. Howick, V.M., Russell, A.J.C., Andrews, T., Heaton, H., Reid, A.J., Natarajan, K., Butungi, H., Metcalf, T., Verzier, L.H., Rayner, J.C., et al. (2019). The Malaria Cell Atlas: Single parasite transcriptomes across the complete *Plasmodium* life cycle. Science *365*. https://doi.org/10.1126/science.aaw2619.

2. Real, E., Howick, V.M., Dahalan, F.A., Witmer, K., Cudini, J., Andradi-Brown, C., Blight, J., Davidson, M.S., Dogga, S.K., Reid, A.J., et al. (2021). A single-cell atlas of *Plasmodium falciparum* transmission through the mosquito. Nat. Commun. *12*, 3196. https://doi.org/10.1038/s41467-021-23434-z.

3. Reid, A.J., Talman, A.M., Bennett, H.M., Gomes, A.R., Sanders, M.J., Illingworth, C.J.R., Billker, O., Berriman, M., and Lawniczak, M.K.N. (2018). Single-cell RNA-seq reveals hidden transcriptional variation in malaria parasites. Elife *7*. https://doi.org/10.7554/eLife.33105.

4. Howick, V.M., Peacock, L., Kay, C., Collett, C., Gibson, W., and Lawniczak, M.K.N. (2022). Single-cell transcriptomics reveals expression profiles of *Trypanosoma brucei* sexual stages. PLoS Pathog *18*, e1010346. https://doi.org/10.1371/journal.ppat.1010346.

5. Briggs, E.M., Rojas, F., McCulloch, R., Matthews, K.R., and Otto, T.D. (2021). Single-cell transcriptomic analysis of bloodstream *Trypanosoma brucei* reconstructs cell cycle progression and developmental quorum sensing. Nat. Commun. *12*, 5268. https://doi.org/10.1038/s41467-021-25607-2.

6. Vigneron, A., O'Neill, M.B., Weiss, B.L., Savage, A.F., Campbell, O.C., Kamhawi, S., Valenzuela, J.G., and Aksoy, S. (2020). Single-cell RNA sequencing of from tsetse salivary glands unveils metacyclogenesis and identifies potential transmission blocking antigens. Proc. Natl. Acad. Sci. U. S. A. *117*, 2613–2621. https://doi.org/10.1073/pnas.1914423117.

7. Briggs, E.M., Marques, C.A., Oldrieve, G.R., Hu, J., Otto, T.D., and Matthews, K.R. (2023). Profiling the bloodstream form and procyclic form cell cycle using single-cell transcriptomics. Elife *12*. https://doi.org/10.7554/eLife.86325.

8. Diaz Soria, C.L., Lee, J., Chong, T., Coghlan, A., Tracey, A., Young, M.D., Andrews, T., Hall, C., Ng, B.L., Rawlinson, K., et al. (2020). Single-cell atlas of the first intra-mammalian developmental stage of the human parasite *Schistosoma mansoni*. Nat. Commun. *11*, 6411. https://doi.org/10.1038/s41467-020-20092-5.

9. Li, P., Nanes Sarfati, D., Xue, Y., Yu, X., Tarashansky, A.J., Quake, S.R., and Wang, B. (2021). Single-cell analysis of *Schistosoma mansoni* identifies a conserved genetic program controlling germline stem cell fate. Nat. Commun. *12*, 485. https://doi.org/10.1038/s41467-020-20794-w.

10. Attenborough, T., Rawlinson, K.A., Diaz Soria, C.L., Ambridge, K., Sankaranarayanan, G., Graham, J., Cotton, J.A., Doyle, S.R., Rinaldi, G., and Berriman, M. (2024). A single-cell atlas of the miracidium larva of reveals cell types, developmental pathways, and tissue architecture. Elife *13*. https://doi.org/10.7554/eLife.95628.

11. Diaz Soria, C.L., Attenborough, T., Lu, Z., Fontenla, S., Graham, J., Hall, C., Thompson, S., Andrews, T.G.R., Rawlinson, K.A., Berriman, M., et al. (2024). Single-cell transcriptomics of the human parasite *Schistosoma mansoni* first intra-molluscan stage

reveals tentative tegumental and stem-cell regulators. Sci Rep *14*, 5974. https://doi.org/10.1038/s41598-024-55790-3.

12. Puckelwaldt, O., Gramberg, S., Ajmera, S., Koepke, J., Samakovlis, C., and Haeberlein, S. (2024). Single-cell transcriptomics identifies a p21-activated kinase important for survival of the zoonotic parasite *Fasciola hepatica*. bioRxiv, 2024.03.26.586785. https://doi.org/10.1101/2024.03.26.586785.

13. Henthorn, C.R., Airs, P.M., Neumann, E.K., and Zamanian, M. (2023). Resolving the origins of secretory products and anthelmintic responses in a human parasitic nematode at single-cell resolution. Elife *12*. https://doi.org/10.7554/eLife.83100.

14. Tyagi, R., Rosa, B.A., Swain, A., Artyomov, M.N., Jasmer, D.P., and Mitreva, M. (2024). Intestinal cell diversity and treatment responses in a parasitic nematode at single cell resolution. BMC Genomics *25*, 1–21. https://doi.org/10.1186/s12864-024-10203-7.

15. Korhonen, P.K., Wang, T., Young, N.D., Byrne, J.J., Campos, T.L., Chang, B.C.H., Taki, A.C., and Gasser, R.B. (2024). Analysis of Haemonchus embryos at single cell resolution identifies two eukaryotic elongation factors as intervention target candidates. Comput. Struct. Biotechnol. J. *23*, 1026–1035. https://doi.org/10.1016/j.csbj.2024.01.008.

16. Pollo, S.M.J., Liu, H., Coria, A.L., Rosin, N., Labit, E., Biernaskie, J., Finney, C.A.M., and Wasmuth, J.D. (2024). A single-cell transcriptomics atlas for the parasitic nematode *Heligmosomoides bakeri*: Extrapolating model organism information to non-model systems. bioRxiv. https://doi.org/10.1101/2024.02.27.582282.

17. Truong, L., Chen, Y.-W., Barrere-Cain, R., Levenson, M.T., Shuck, K., Xiao, W., da Veiga Beltrame, E., Panter, B., Reich, E., Sternberg, P.W., et al. (2023). Single-nucleus resolution mapping of the adult *C. elegans* and its application to elucidate inter- and trans-generational response to alcohol. Cell Rep. *42*. https://doi.org/10.1016/j.celrep.2023.112535.

18. Levenson, M.T., Barrere-Cain, R., Truong, L., Chen, Y.-W., Shuck, K., Panter, B., Reich, E., Yang, X., and Allard, P. (2023). Protocol for nuclear dissociation of the adult *C. elegans* for single-nucleus RNA sequencing and its application for mapping environmental responses. STAR Protocols *4*, 102756. https://doi.org/10.1016/j.xpro.2023.102756.

19. Stephenson, E. (2023). Nuclei isolation from frozen tissue (protocols.io) https://doi.org/10.17504/protocols.io.8epv5x6wjg1b/v1.

20. G Martelotto, L., and Martelotto, L. (2020). “Frankenstein” protocol for nuclei isolation from fresh and frozen tissue for snRNAseq v3. (ZappyLab, Inc.). https://doi.org/10.17504/protocols.io.bqxymxpw https://doi.org/10.17504/protocols.io.bqxymxpw.

21. Regev, A., Teichmann, S.A., Lander, E.S., Amit, I., Benoist, C., Birney, E., Bodenmiller, B., Campbell, P., Carninci, P., Clatworthy, M., et al. (2017). The Human Cell Atlas. Elife *6*. https://doi.org/10.7554/eLife.27041.

22. Madissoon, E., Wilbrey-Clark, A., Miragaia, R.J., Saeb-Parsy, K., Mahbubani, K.T., Georgakopoulos, N., Harding, P., Polanski, K., Huang, N., Nowicki-Osuch, K., et al. (2019). scRNA-seq assessment of the human lung, spleen, and esophagus tissue stability after cold preservation. Genome Biol *21*, 1. https://doi.org/10.1186/s13059-019-1906-x.

23. Can I use an alternative RNase inhibitor part number? (10x Genomics).

24. International Helminth Genomes Consortium (2018). Comparative genomics of the major parasitic worms. Nat. Genet. *51*, 163–174. https://doi.org/10.1038/s41588-018-0262-1.

25. Hedgecock, E.M., and White, J.G. (1985). Polyploid tissues in the nematode *Caenorhabditis elegans*. Dev Biol *107*, 128–133. https://doi.org/10.1016/0012-1606(85)90381-1.

26. Rosenberg, A.B., Roco, C.M., Muscat, R.A., Kuchina, A., Sample, P., Yao, Z., Graybuck, L.T., Peeler, D.J., Mukherjee, S., Chen, W., et al. (2018). Single-cell profiling of the developing mouse brain and spinal cord with split-pool barcoding. Science *360*, 176–182. https://doi.org/10.1126/science.aam8999.

27. Roux, A.E., Yuan, H., Podshivalova, K., Hendrickson, D., Kerr, R., Kenyon, C., and Kelley, D. (2023). Individual cell types in C. elegans age differently and activate distinct cell-protective responses. Cell Rep. *42*, 112902. https://doi.org/10.1016/j.celrep.2023.112902.

28. Doyle, S.R. (2022). Improving helminth genome resources in the post-genomic era. Trends Parasitol. *38*, 831–840. https://doi.org/10.1016/j.pt.2022.06.002.

29. Wu, H., Kirita, Y., Donnelly, E.L., and Humphreys, B.D. (2019). Advantages of Single-Nucleus over Single-Cell RNA Sequencing of Adult Kidney: Rare Cell Types and Novel Cell States Revealed in Fibrosis. J. Am. Soc. Nephrol. *30*, 23–32. https://doi.org/10.1681/ASN.2018090912.

30. van den Brink, S.C., Sage, F., Vértesy, Á., Spanjaard, B., Peterson-Maduro, J., Baron, C.S., Robin, C., and van Oudenaarden, A. (2017). Single-cell sequencing reveals dissociation-induced gene expression in tissue subpopulations. Nat. Methods *14*, 935–936. https://doi.org/10.1038/nmeth.4437.

31. Slyper, M., Porter, C.B.M., Ashenberg, O., Waldman, J., Drokhlyansky, E., Wakiro, I., Smillie, C., Smith-Rosario, G., Wu, J., Dionne, D., et al. (2020). A single-cell and single-nucleus RNA-Seq toolbox for fresh and frozen human tumors. Nat Med *26*, 792–802. https://doi.org/10.1038/s41591-020-0844-1.

32. O'Sullivan, J.D.B., Cruickshank, S.M., Withers, P.J., and Else, K.J. (2021). Morphological variability in the mucosal attachment site of *Trichuris muris* revealed by X-ray microcomputed tomography. Int J Parasitol *51*, 797–807. https://doi.org/10.1016/j.ijpara.2021.04.006.

33. Podbilewicz, B. (2006). Cell fusion. In WormBook: The online review of C. elegans biology, J. M. Kramer and D. G. Moerman, eds. (The C. elegans Research Community).

34. Cantacessi, C., Campbell, B.E., Young, N.D., Jex, A.R., Hall, R.S., Presidente, P.J.A., Zawadzki, J.L., Zhong, W., Aleman-Meza, B., Loukas, A., et al. (2010). Differences in transcription between free-living and CO2-activated third-stage larvae of *Haemonchus contortus*. BMC Genomics *11*, 266. https://doi.org/10.1186/1471-2164-11-266.

35. Cao, J., Packer, J.S., Ramani, V., Cusanovich, D.A., Huynh, C., Daza, R., Qiu, X., Lee, C., Furlan, S.N., Steemers, F.J., et al. (2017). Comprehensive single-cell transcriptional profiling of a multicellular organism. Science *357*, 661–667. https://doi.org/10.1126/science.aam8940.

36. Alfieri, J.M., Wang, G., Jonika, M.M., Gill, C.A., Blackmon, H., and Athrey, G.N. (2022). A Primer for Single-Cell Sequencing in Non-Model Organisms. Genes *13*. https://doi.org/10.3390/genes13020380.

37. Evercode Fixation and WT v2 User Guides (2023). (Parse Biosciences).

38. Srivastava, N., Nader, G.P. de F., Williart, A., Rollin, R., Cuvelier, D., Lomakin, A., and Piel, M. (2021). Nuclear fragility, blaming the blebs. Curr. Opin. Cell Biol. *70*, 100–108. https://doi.org/10.1016/j.ceb.2021.01.007.

39. Wakelin, D. (1967). Acquired immunity to *Trichuris muris* in the albino laboratory mouse. Parasitology *57*, 515–524. https://doi.org/10.1017/s0031182000072395.

40. White, E.C., Houlden, A., Bancroft, A.J., Hayes, K.S., Goldrick, M., Grencis, R.K., and Roberts, I.S. (2018). Manipulation of host and parasite microbiotas: Survival strategies during chronic nematode infection. Sci Adv *4*, eaap7399. https://doi.org/10.1126/sciadv.aap7399.

41. Duque-Correa, M.A., Karp, N.A., McCarthy, C., Forman, S., Goulding, D., Sankaranarayanan, G., Jenkins, T.P., Reid, A.J., Cambridge, E.L., Ballesteros Reviriego, C., et al. (2019). Exclusive dependence of IL-10Rα signalling on intestinal microbiota homeostasis and control of whipworm infection. PLoS Pathog. *15*, e1007265. https://doi.org/10.1371/journal.ppat.1007265.

42. Hu, P., Fabyanic, E., Kwon, D.Y., Tang, S., Zhou, Z., and Wu, H. (2017). Dissecting Cell-Type Composition and Activity-Dependent Transcriptional State in Mammalian Brains by Massively Parallel Single-Nucleus RNA-Seq. Mol. Cell *68*, 1006–1015.e7. https://doi.org/10.1016/j.molcel.2017.11.017.

43. Habib, N., Li, Y., Heidenreich, M., Swiech, L., Avraham-Davidi, I., Trombetta, J.J., Hession, C., Zhang, F., and Regev, A. (2016). Div-Seq: Single-nucleus RNA-Seq reveals dynamics of rare adult newborn neurons. Science *353*, 925–928. https://doi.org/10.1126/science.aad7038.

44. Habib, N., Avraham-Davidi, I., Basu, A., Burks, T., Shekhar, K., Hofree, M., Choudhury, S.R., Aguet, F., Gelfand, E., Ardlie, K., et al. (2017). Massively parallel single-nucleus RNA-seq with DroNc-seq. Nat. Methods *14*, 955–958. https://doi.org/10.1038/nmeth.4407.

45. Lake, B.B., Ai, R., Kaeser, G.E., Salathia, N.S., Yung, Y.C., Liu, R., Wildberg, A., Gao, D., Fung, H.-L., Chen, S., et al. (2016). Neuronal subtypes and diversity revealed by single-nucleus RNA sequencing of the human brain. Science *352*, 1586–1590. https://doi.org/10.1126/science.aaf1204.

46. Lacar, B., Linker, S.B., Jaeger, B.N., Krishnaswami, S., Barron, J., Kelder, M., Parylak, S., Paquola, A., Venepally, P., Novotny, M., et al. (2016). Nuclear RNA-seq of single neurons reveals molecular signatures of activation. Nat. Commun. *7*, 11022. https://doi.org/10.1038/ncomms11022.

47. Nadelmann, E.R., Gorham, J.M., Reichart, D., Delaughter, D.M., Wakimoto, H., Lindberg, E.L., Litviňukova, M., Maatz, H., Curran, J.J., Ischiu Gutierrez, D., et al. (2021). Isolation of Nuclei from Mammalian Cells and Tissues for Single-Nucleus Molecular Profiling. Curr Protoc *1*, e132. https://doi.org/10.1002/cpz1.132.

48. Ewels, P., Magnusson, M., Lundin, S., and Käller, M. (2016). MultiQC: summarize analysis results for multiple tools and samples in a single report. Bioinformatics *32*,

3047–3048. https://doi.org/10.1093/bioinformatics/btw354.

49. Doyle, S.R., Tracey, A., Laing, R., Holroyd, N., Bartley, D., Bazant, W., Beasley, H., Beech, R., Britton, C., Brooks, K., et al. (2020). Genomic and transcriptomic variation defines the chromosome-scale assembly of *Haemonchus contortus*, a model gastrointestinal worm. Commun Biol *3*, 656. https://doi.org/10.1038/s42003-020-01377-3.

50. Foth, B.J., Tsai, I.J., Reid, A.J., Bancroft, A.J., Nichol, S., Tracey, A., Holroyd, N., Cotton, J.A., Stanley, E.J., Zarowiecki, M., et al. (2014). Whipworm genome and dual-species transcriptome analyses provide molecular insights into an intimate host-parasite interaction. Nat. Genet. *46*, 693–700. https://doi.org/10.1038/ng.3010.

51. Germain, P.-L., Lun, A., Meixide, C.G., Macnair, W., and Robinson, M.D. (2022). Doublet identification in single-cell sequencing data using *scDblFinder*. F1000Research *10*, 979. https://doi.org/10.12688/f1000research.73600.2.

52. Howe, K.L., Bolt, B.J., Shafie, M., Kersey, P., and Berriman, M. (2017). WormBase ParaSite - a comprehensive resource for helminth genomics. Mol Biochem Parasitol *215*, 2–10. https://doi.org/10.1016/j.molbiopara.2016.11.005.

53. Kuleshov, M.V., Jones, M.R., Rouillard, A.D., Fernandez, N.F., Duan, Q., Wang, Z., Koplev, S., Jenkins, S.L., Jagodnik, K.M., Lachmann, A., et al. (2016). Enrichr: a comprehensive gene set enrichment analysis web server 2016 update. Nucleic Acids Res *44*, W90–W97. https://doi.org/10.1093/nar/gkw377.

54. Chen, E.Y., Tan, C.M., Kou, Y., Duan, Q., Wang, Z., Meirelles, G.V., Clark, N.R., and Ma'ayan, A. (2013). Enrichr: interactive and collaborative HTML5 gene list enrichment analysis tool. BMC Bioinformatics *14*, 128. https://doi.org/10.1186/1471-2105-14-128.

55. Kolberg, L., Raudvere, U., Kuzmin, I., Adler, P., Vilo, J., and Peterson, H. (2023). g:Profiler-interoperable web service for functional enrichment analysis and gene identifier mapping (2023 update). Nucleic Acids Res *51*, W207–W212. https://doi.org/10.1093/nar/gkad347.